INTERNATIONAL JOURNAL FOR NUMERICAL METHODS IN FLUIDS
Int. J. Numer. Meth. Fluids **29**: 75–95 (1999)

A GENERAL APPROACH FOR COMPUTING UNSTEADY 3D THIN LIFTING AND/OR PROPULSIVE SYSTEMS DERIVED FROM A COMPLETE THEORY

A. LEROY* AND PH. DEVINANT

Laboratoire de Mécanique et Energétique, Ecole Supérieure de l'Energie et des Matériaux, Université d'Orléans, Rue Léonard de Vinci, F-45072 Orléans Cedex 2, France

SUMMARY

This paper presents the basis of a numerical method for unsteady aerodynamic computation around thin lifting and/or propulsive systems with arbitrary variable geometries, involving the velocity field, the velocity potential, the pressure field and the wake characteristics (geometry and vortex strength). Most of the corresponding theory actually stems from the unsteady wake model established by Mudry, in which the wake is considered to be a median layer, characterized by a pair of functions on which Mudry founded the concept of continuous vortex particle. The governing relations of the continuous problem are then the flow tangency condition, the wake integro-differential evolution equation, and a flow regularity condition at the trailing edge. This constitutes a rigorous and complete theoretical formulation of this problem, from which a discretization scheme and a numerical method of solution are derived. The view of the vortex wake is similar to the one in the classical vortex lattice approaches, but uses a discrete vortex particle concept, particularly well suited for the prediction of the unsteady wake deformation. This, together with the continuous theory, ensures the computing method compares favorably with the classical methods in terms of flexibility and computing costs. In order to demonstrate the capabilities of the present method, the calculation of flapping wings of variable geometry is also presented.

KEY WORDS: potential flow; unsteady aerodynamics; wake geometry; 3D wakes; vortex particles; numerical simulations

1. INTRODUCTION

Analysis of complex 3D configurations requires computational methods for unsteady aerodynamics, particularly for the prediction of wake distortions and time variations. For example, in the case of a two-element airfoil, the wake of the main airfoil is very close to the upper surface of the trailing edge flap. Similarly, estimated rotorcraft vortex wake shapes can shed light on one of the most complex problems associated with a helicopter flight, namely the blade–vortex interaction. For such developments, an improved vortex wake model is needed so that wake shedding and time variations can be analyzed precisely.

In the general framework of non-separated flows of inviscid incompressible irrotational fluid, wakes from lifting and/or propulsive systems are represented by vortex sheets and are

* Correspondence to: Laboratoire de Mécanique et Energétique, Ecole Supérieure de l'Energie et des Matériaux, Université d'Orléans, Rue Léonard de Vinci, F-45072 Orléans Cedex 2, France. Tel: + 33 238417050; Fax: + 33 238417383; E-mail: annie.leroy@univ-orleans.fr

CCC 0271–2091/99/010075–21$17.50

Received September 1997
Revised January 1998

discretized by an arrangement of vortex elements. Two broad types of methods currently exist for computing these flows, differing in the way they consider the wake.

The first considers the wake as a distribution of doublet type singularities. The wakes are usually approximated by trapezoidal elements. When the doublet density is assumed to be constant, this is equivalent to closed vortex rings [1] and therefore corresponds to a vortex lattice approximation. These vortex lattice elements move with time according to the local velocity field. Computer developments have allowed direct numerical approach of 3D non-linearized problems of this kind; e.g. References [2–6].

The second type of methods considers the wake to be sufficiently thick, so that it is represented by volume vortex particles, e.g. References [7–10]. These methods are based on a volume discretization of the vortex vector, i.e. the velocity curl. To follow the time variation of a discrete distribution of fluid particles in the wake, with each particle supporting this vortex vector, a Lagrangian integro-differential formulation based on the Helmholtz equation is used.

In fact, both approaches are more or less based on discrete formulations and are not always well founded in theory. The first approach, as it is built on an already discretized view of the problem, entirely overlooks the theoretical problem of wake variation with time. Consequently, this can lead to numerical problems when the wake distortions are large. Nevertheless, it is used often because of its competitive numerical capabilities in terms of flexibility and computational costs. Although the vortex particle model seems to offer the possibility of developing a strictly accurate deformation problem, it has the drawback of high-cost numerical algorithms, especially for treating the Helmholtz equation using complex regularized schemes [10].

This paper uses a general non-linear theory for time-dependent problems of a lifting and/or propulsive system of variable geometry in arbitrary motion in a potential flow. The problem is first formulated in theory with no reference to any discrete approach and mostly relates to the wake model established by Mudry [11]. An exact continuous scheme is developed from this, focusing mainly on the wake shedding and time deformation, so as to develop an efficient computational scheme for calculating the unsteady airloads and predicting the wake geometry. This leads to numerical tools offering the flexibility and low computational costs of the first approach presented above, based on a rigorous theory of the deforming unsteady wake problem.

Most of this work stems from a thesis written for the *Laboratoire de Mécanique et d'Energétique* at the Université d'Orléans [15].

2. GENERAL FRAMEWORK OF THE PROBLEM

A lifting–propulsive system consists of 3D elements of arbitrary geometry driven by arbitrary motions. In many cases, these elements, such as blades of helicopter rotors, rotating propellers and wind turbines, as well as flapping wings, can be considered as thin. That is why the elements dealt with here are assumed to be surfaces.

In the case of a viscous fluid, the flow is irrotational over the entire flowfield, except at the body's solid boundaries and in the wake, where it results from the mixture of the two boundary layers from the lower and upper surfaces of the wing. In the case of evanescent viscosity, the boundary layers and wake are thin and in the limiting case of an inviscid flow, the wake has to be considered as an infinitely thin layer, and more particularly as the union of two distinct fluid surfaces issuing from the lower and upper surfaces of the wing (Figure 1). The two boundary layers no longer exist. The boundary condition of fluid adherence is

replaced by a flow tangency condition. Therefore, the wake must be considered as a single surface of two superimposed distinct fluid surfaces, coming from the two sides of the wing's edge, and remaining in contact with each other after leaving it. Then, for an inviscid fluid, the wake is a slip surface, and as it cannot sustain pressure differences, the wake is a discontinuity surface for the tangential velocity component of the fluid particles located on both sides of this surface.

Consider a variable-geometry thin airfoil A in motion relative to a surrounding fluid and the user-defined shedding lines $\Im$ (trailing edge in general) of its wake Σ. The fluid is assumed to be inviscid and incompressible over the entire irrotational flow field, excluding the wing and its wake. Therefore, a velocity potential ϕ can be defined in an inertial frame of reference that will satisfy Laplace's equation:

$$\Delta\phi = 0, \tag{1}$$

and will be subject to the following boundary conditions:

- flow tangency, requiring zero normal velocity across the wing,
- quiescent freestream fluid,
- Kutta–Joukowski condition of smooth flow off the shedding edge,
- dynamical condition of pressure continuity across the wake.

By use of Green's theorem, it can be shown that the velocity potential on and outside the surfaces A and Σ, is given by

$$P \in \mathbb{R}^3 \mapsto \phi(P) = -\frac{1}{4\pi}\iint_A \sigma(M)\frac{\vec{r}\cdot\vec{n}_M}{r^3}\,\mathrm{d}S - \frac{1}{4\pi}\iint_\Sigma \mu(M)\frac{\vec{r}\cdot\vec{n}_M}{r^3}\,\mathrm{d}S, \tag{2}$$

where σ and μ are, respectively, the doublet strengths over the entire surfaces A and Σ. σ and μ are equal to the opposite of the velocity potential discontinuity across A and Σ: $\sigma = -[\phi]_A$

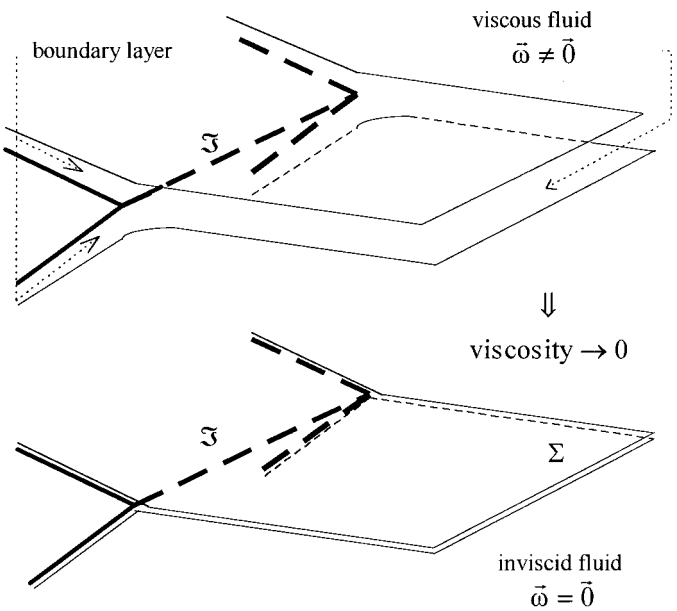

Figure 1. Wake in viscous fluid and in inviscid fluid.

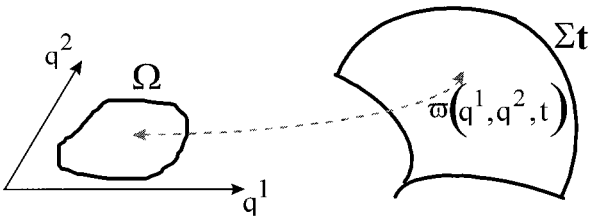

Figure 2. Parametrisation of a surface.

and $\mu = -[\phi]_\Sigma$. P is a field point, $\vec{n}_M$ is the outward normal in M, and $\vec{r} = \vec{MP}$, $r = \|\vec{r}\|$. For P on A or Σ, the first or second integral in Equation (2), respectively, is singular. It is a Cauchy integral which can be properly evaluated in the principal value sense. This doublet distribution solution automatically fulfills the boundary condition of quiescent fluid at infinity.

The derivation of the velocity potential induced by such a general doublet distribution on any surface S at any point in the field, is

$$\vec{\text{grad}}\ \phi = -\frac{1}{4\pi}\iint_S \mu(M)\vec{\text{grad}}\left(\frac{\vec{r}\cdot\vec{n}_M}{r^3}\right)\text{d}S. \tag{3}$$

The resulting formulation is then [11]

$$\vec{\text{grad}}\ \phi = -\frac{1}{4\pi}\iint_S \frac{(\vec{n}_M \wedge \vec{\nabla}\mu(M)) \wedge \vec{r}}{r^3}\,\text{d}S + \frac{1}{4\pi}\int_{\partial S} \mu(M)\vec{\text{grad}}_M\left(\frac{1}{r}\right) \wedge \text{d}\vec{M}, \tag{4}$$

in which ∂S indicates the oriented edge of S; $\vec{\nabla}$ is the surface gradient of a scalar quantity defined on S, relative to a local frame associated with S; whereas $\vec{\text{grad}}_M$ is the gradient of a scalar quantity defined in the 3D domain $\mathbb{R}^3$ and evaluated at the point M of S. This expression shows the usual two terms. The first is a surface integral, involving the surface gradient of the doublet density distribution on the surface. The second is a curvilinear integral involving the value of doublet density distribution along the edge of the surface. It can be noted that the second term vanishes when either S is a closed surface or μ is equal to zero at any free edge of S. In the case of an irrotational flow, and if S is a singular surface for the velocity field, e.g. a thin wake, Reference [11] showed that for Equation (4) to be the induced velocity by this double-layer surface S, the second term in Equation (4) must be equal to zero. A wake is not a closed surface, therefore the doublet density μ must be zero at any free edge of S.

In case S is the union of a thin airfoil A and its thin wake Σ, μ is zero at the free edge. Then, the second term of Equation (4) vanishes, but it does not vanish when only a part of S is considered (A and Σ separately considered, a panel resulting from a discretization of S, . . .).

3. GENERAL THEORETICAL FORMULATION

3.1. Unsteady wake and the concept of vortex particles

From the concept of slip surface, Mudry [12] developed a general theory for unsteady wakes, considered as vortex sheets, in the general framework of inviscid incompressible fluid and irrotational flow. The main results of his theory follow.

As the wake Σ is a surface, Mudry introduced a two-parameter description of its geometrical shape, as shown in Figure 2. For the points N of the wake Σ, and O the origin of the co-ordinate system in relation to an inertial frame, any parametrisation $\vec{\varpi}$ is defined as

$$\begin{cases}(q^1, q^2)\in\Omega\subset\mathbb{R}^2\\ N=(x_1, x_2, x_3)\in\mathbb{R}^3\end{cases}\qquad t\in I\subset\mathbb{R}\mapsto\vec{ON}=\vec{\varpi}(q^1, q^2, t)\in\Sigma. \tag{5}$$

As the wake is a superimposition of two distinct fluid surfaces, it could be described by two parametrisations referring to these two surfaces: $\vec{\varpi}^+$ and $\vec{\varpi}^-$, noting $\ll + \gg$ for the upper surface and $\ll - \gg$ for the lower. But as Mudry founded his theory on the median layer concept, which Helmholtz first introduced in terms of median velocity, Mudry characterized the vortex sheet representing the wake, by the non-unique pair of functions [13]

– the 'median parametrisation', $\vec{\varpi}$, such that $\vec{\varpi}$ verifies the following wake time variation equation:

$$\frac{\partial\vec{\varpi}(q^1, q^2, t)}{\partial t}=\frac{\vec{U}^+ + \vec{U}^-}{2}=\vec{U}^*(\vec{\varpi}(q^1, q^2, t)), \tag{6}$$

where $\vec{U}^*$ is the median velocity field due to the flow, i.e. the half-sum of the two fluid surfaces velocities. Then, $\vec{\varpi}$ determines the geometrical shape of the vortex sheet and its deformation.

– the associated 'median vortex density', $\vec{\gamma}$, that describes the vortex sheet strength. It is a function of the local velocity jump and of the geometrical description of the wake carried out by $\vec{\varpi}$:

$$\vec{\gamma}(q^1, q^2, t)=\vec{N}\wedge[\vec{U}]=\left[\frac{\partial\vec{\varpi}}{\partial q^1}\wedge\frac{\partial\vec{\varpi}}{\partial q^2}\right]\wedge[\vec{U}]=\gamma^1\frac{\partial\vec{\varpi}}{\partial q^1}+\gamma^2\frac{\partial\vec{\varpi}}{\partial q^2}, \tag{7}$$

where $[\vec{U}]=\vec{U}^+ - \vec{U}^-$ indicates the velocity jump through the surface considered.

$(\vec{\varpi}, \vec{\gamma})$ clearly states the concept of continuous vortex particle to represent the wake with no discretization. Any vortex particle position can be defined by the point $N: t\mapsto\vec{ON}=\vec{\varpi}(q^1, q^2, t)$.

From the wake time variation equation (6), Mudry demonstrated the fundamental time-conservation property for the two contravariant components γ^α $(\alpha=1, 2)$ of the median vortex density. This property is derived from the choice of the parametrisation $\vec{\varpi}$ together with the pressure continuity condition through the wake.

Since the flow is assumed to be irrotational, a function G, the surface discontinuity potential, can be defined as being equivalent to the potential jump through Σ: $G=\phi^+ - \phi^- =[\phi]$. Mudry has shown that $\vec{\gamma}$ is derived from G, because G is given by

$$[\vec{U}]=\vec{\nabla}G=\vec{\nabla}[\phi], \tag{8}$$

where $\vec{\nabla}$ is a surface gradient. Thus, $\gamma^1=-\partial G/\partial q^2$ and $\gamma^2=\partial G/\partial q^1$, and G does not depend on time.

Then, using G and $\vec{\gamma}$, the velocity potential and the velocity induced by the vortex sheet Σ take the forms

$$\phi(x, t)=\frac{1}{4\pi}\iint_\Omega G(q^1, q^2)\frac{(\vec{x}-\vec{\varpi})\cdot(\partial_1\vec{\varpi}\wedge\partial_2\vec{\varpi})}{\|\vec{x}-\vec{\varpi}\|^3}\,\mathrm{d}q^1\,\mathrm{d}q^2, \tag{9}$$

$$\vec{U}(x, t)=\vec{\mathrm{grad}}\;\phi(x, t)=\frac{1}{4\pi}\iint_\Omega\frac{\vec{\gamma}\wedge\vec{r}}{r^3}\,\mathrm{d}q^1\,\mathrm{d}q^2-\frac{1}{4\pi}\int_{\partial\Omega}G\,\vec{\mathrm{grad}}_x\left(\frac{1}{r}\right)\wedge\vec{\mathrm{d}\xi}. \tag{10}$$

The integration domain is a known range defined by the definition plane (q^1, q^2) of the parametrisation $\vec{\varpi}$, and does not explicitly depend on time.

The wake shedding is taken into account by specifying that q^1 is equal to the shedding edge parameter linked to a shedding edge representation: q, and q^2 to the shedding time: τ,

$$q^1 = q, \quad q \in J \subset \mathbb{R}, \qquad q^2 = \tau, \quad \tau \in [0, t]. \tag{11}$$

Thus, from a Lagrangian representation $\vec{h}(q, t)$ of the shedding edge $\mathfrak{I}$ in the inertial frame:

$$\vec{OP} = \vec{h}(q, t), \tag{12}$$

the shedding condition of the wake can be defined as

$$\vec{\varpi}(q, \tau, \tau) = \vec{h}(q, \tau). \tag{13}$$

The shedding relative velocity $\vec{V}_{\text{re}}$, which is the velocity of the vortex particle at and relative to $\mathfrak{I}$, is derived from Equation (13), as

$$\vec{V}_{\text{re}} = \left(\frac{\partial \vec{\varpi}(q, \tau, \tau)}{\partial t} \right)_e - \frac{\partial \vec{h}(q, t)}{\partial t}, \tag{14}$$

where $\partial \vec{h}/\partial t$ is actually the absolute velocity of the shedding edge points and $(\partial \vec{\varpi}/\partial t)_e$ is the absolute velocity of the vortex particle being shed.

Studying the shedding mechanism, Mudry showed that a shedding plane related to a pair (q, τ) exists at every instant, defined by the two vectors $\vec{V}_{\text{re}}$ and $\partial \vec{h}/\partial q$. In the case of a thin airfoil it can be shown that this plane is tangent to the airfoil at $\mathfrak{I}$.

Because of the time-conservation property of the two contravariant components of the vortex density, these components are determined when the particle is shed. Therefore, the problem of computing the wake, which consists of determining the position and density of the vortex particles once shed, reduces to solving the integro-differential equation (6):

$$\frac{\partial \vec{\varpi}(q, \tau, t)}{\partial t} = \frac{1}{4\pi} \iint_{\Omega} \frac{\vec{\gamma}(q', \tau') \wedge (\vec{\varpi}(q, \tau, t) - \vec{\varpi}(q', \tau', t))}{\|\vec{\varpi}(q, \tau, t) - \vec{\varpi}(q', \tau', t)\|^3} \, \mathrm{d}q' \, \mathrm{d}\tau' + \vec{U}_A(\vec{\varpi}(q, \tau, t)). \tag{15}$$

Equation (15) governs the new position of the vortex particles at every moment. Here, $\vec{U}_A$ represents the velocity field induced by the airfoil.

3.2. General non-linear equations

Let a variable-geometry thin airfoil A be considered. A and its wake Σ, shed at the edge $\mathfrak{I}$, are vortex sheets in an inviscid fluid. The geometrical shape is known for the airfoil, whereas it is unknown for the wake. From Mudry's general theory, the general problem of non-linear unsteady 3D flow around a thin airfoil can then be formulated exactly.

As for the wake, a parametrisation $\vec{\chi}$, defined in the inertial frame, and an associated vortex density $\vec{\delta}$ related to the airfoil are introduced:

$$M \in A \Leftrightarrow \vec{OM} = \vec{\chi}(\theta^1, \theta^2, t), \quad (\theta^1, \theta^2) \in \Theta \subset \mathbb{R}^2, \tag{16}$$

$$\vec{\delta}(\theta^1, \theta^2, t) = \left(\frac{\partial \vec{\chi}}{\partial \theta^1} \wedge \frac{\partial \vec{\chi}}{\partial \theta^2} \right) \wedge [\vec{U}] = \delta^1 \frac{\partial \vec{\chi}}{\partial \theta^1} + \delta^2 \frac{\partial \vec{\chi}}{\partial \theta^2}. \tag{17}$$

The contravariant components (δ^1, δ^2) are dependent on time and are governed by the flow tangency condition on A. They are derived from K, the discontinuity potential on A, given by

$$[\vec{U}] = \vec{\nabla} K = \vec{\nabla}[\phi]. \tag{18}$$

H, the discontinuity potential on the union of A and Σ ($H = G$ on Σ, $H = K$ on A), must be equal to zero on the borders of A and Σ, excluding their common border $\mathfrak{I}$. Through $\mathfrak{I}$, the variations of H will be governed by the Kutta–Joukowsky condition.

When treating time-dependent motion of bodies, the selection of the co-ordinate systems becomes very important. It is useful to describe the unsteady motion of the airfoil in an airfoil-fixed frame $R = (O'; x, y, z)$, as shown in Figure 3. The motion of R corresponds to the motion of the rigid airfoil. It is then prescribed in an inertial frame of reference $R_G = (O; X, Y, Z)$ and is assumed to be known. The kinematic velocity $\vec{V}_E$ of an airfoil point, as viewed in the inertial frame, is given by

$$V_E = \vec{V}_{O'} + \vec{\Omega} \wedge \vec{r}, \tag{19}$$

where $\vec{V}_{O'} = (\partial X_{O'}/\partial t, \partial Y_{O'}/\partial t, \partial Z_{O'}/\partial t)$ is the velocity of O', $\vec{r}$ is the position vector in the (x, y, z) system and $\vec{\Omega}$ is the rate of rotation of the airfoil-fixed frame. In order to define $\vec{V}_E$ in the airfoil-fixed frame, a transformation between these two co-ordinate systems must be established.

An additional relative motion within the (x, y, z) system describes the variable geometry of the airfoil (flap deflections, time variation of twist, etc.) in addition to the average motion of the airfoil. Thus the deformation velocity in the airfoil-fixed frame is defined as

$$\vec{V}_D = \frac{\partial \vec{\chi}}{\partial t}. \tag{20}$$

In the case of a rigid airfoil, $\vec{\chi}(\theta^1, \theta^2, t)$ and $\vec{h}(q, t)$ do not depend on time, and this velocity vanishes.

Figure 4 shows how the physical problem is then formulated in two domains, respectively, related to the definition plane of the parametrisations $\vec{\varpi}$ and $\vec{\chi}$. This is one of the original features of this approach, as the problem is formulated and solved for both vortex sheets (airfoil and wake) in their respective 2D parametrisation planes.

When looking at the velocities induced (Equation (4)) by each surface A and Σ considered independently, note that both integrals are singular at their common edge $\Im$. Therefore, the joining of these two sheets implies some condition on their characteristics so that the resulting fluid velocity field is no longer singular across $\Im$, to insure a regular fluid flow (singularity removal procedure). This has been thoroughly examined in References [14] and [15], and the resulting Kutta–Joukowsky condition in the case of a thin airfoil has been formulated explicitly. The conditions for the fluid velocity to be regular across $\Im$ may then be readily expressed as

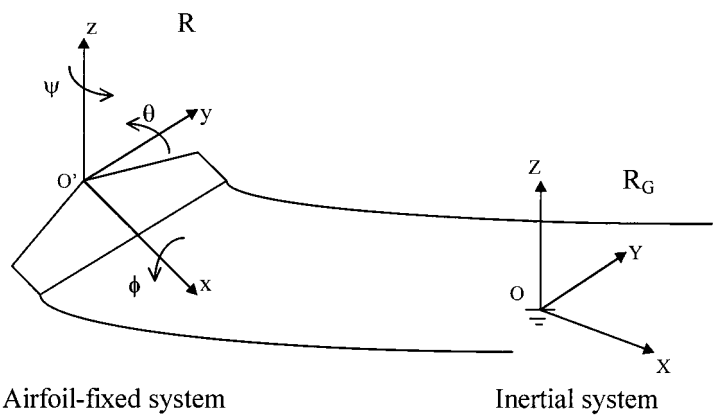

Figure 3. Airfoil-fixed frame R and Galilean frame R_G.

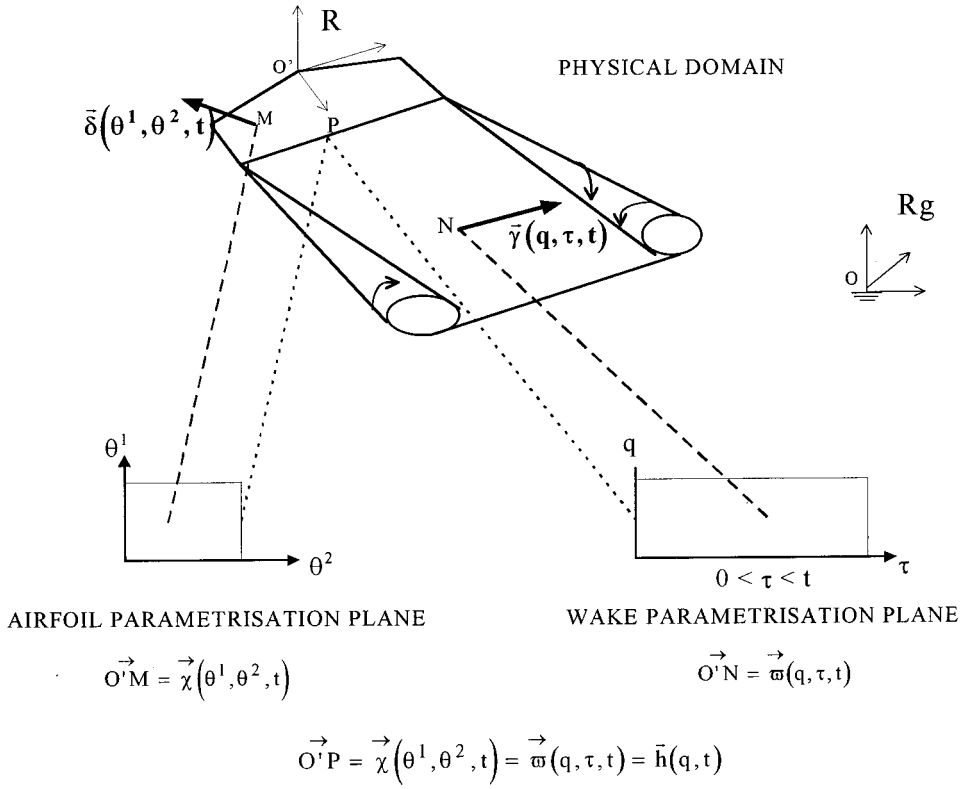

Figure 4. Physical field and parametrisation planes.

$$\text{(i)}\ K=G, \qquad \text{(ii)}\ \frac{\partial K}{\partial v}=\frac{\partial G}{\partial v}, \tag{21}$$

where $\vec{v}$ is the geodesic normal vector to $\Im$ (in a common tangent plane to A and Σ). This means that the potential jump $[\phi]=H$, and the normal (to $\Im$) component $\partial[\phi]/\partial v=\partial H/\partial v$ of its surface gradient must be continuous across $\Im$. The first condition (i) is, in fact, the Kutta–Joukowsky condition considered in practice in the classical vortex lattice approaches [3–6]. But this should only apply, from a strict theoretical view point, to steady linearized flows around airfoils with unswept trailing edges. On an other hand, as soon as we have steady flows with swept trailing edges or unsteady flows for any trailing edge sweep, a strict theoretical approach also has to consider the gradient normal component.

The governing equations of the problem contain ϕ, denoted φ in airfoil-fixed frame, $\vec{U}$, p defined in $D\times I$, $(\vec{\varpi},\vec{\gamma})$ related to Σ and H. These equations are expressed in the airfoil-fixed frame.

- In D/Σ:
  Irrotational flow of an inviscid incompressible fluid:

$$\vec{U}=\vec{\text{grad}}\,\varphi, \qquad \Delta\varphi=0. \tag{22}$$

  Bernoulli's equation:

$$\frac{p_\infty - p}{\rho} = \frac{1}{2}\vec{U}^2 + \frac{\partial \varphi}{\partial t} - \vec{V}_E \cdot \vec{U}. \tag{23}$$

- On A:
  Flow tangency condition:

$$\vec{U} \cdot \vec{n} = (\vec{V}_E + \vec{V}_D) \cdot \vec{n}. \tag{24}$$

- Through $\Im$ ($t = \tau$):
  Shedding condition:

$$\vec{h}(q, t) = \vec{\varpi}(q, t, t). \tag{25}$$

  Shedding relative velocity:

$$\vec{V}_{\text{re}} = \left(\frac{\partial \vec{\varpi}}{\partial t}\right)_e - \frac{\partial \vec{h}}{\partial t}. \tag{26}$$

  Kutta–Joukowsky condition:

$$K = G \quad \text{and} \quad \frac{\partial K}{\partial v} = \frac{\partial G}{\partial v}. \tag{27}$$

- On Σ:
  Zero pressure jump:

$$[p] = 0. \tag{28}$$

  Wake time variation equation:

$$\begin{aligned} &\frac{\partial \vec{\varpi}(q, \tau, t)}{\partial t} + \vec{V}_E(\vec{\varpi}(q, \tau, t), t) \\ &= \frac{1}{4\pi} \iint_\Theta \frac{\vec{\delta}(\theta^1, \theta^2, t) \wedge (\vec{\varpi}(q, \tau, t) - \vec{\chi}(\theta^1, \theta^2, t))}{\|\vec{\varpi}(q, \tau, t) - \vec{\chi}(\theta^1, \theta^2, t)\|^3} \, \mathrm{d}\theta^1 \, \mathrm{d}\theta^2 \\ &\quad + \frac{1}{4\pi} \int_0^t \int_J \frac{\vec{\gamma}(q', \tau') \wedge (\vec{\varpi}(q, \tau, t) - \vec{\varpi}(q', \tau', t))}{\|\vec{\varpi}(q, \tau, t) - \vec{\varpi}(q', \tau', t)\|^3} \, \mathrm{d}q' \, \mathrm{d}\tau'. \end{aligned} \tag{29}$$

Here the curvilinear integral of Equation (10) disappears because of both the Kutta–Joukowsky condition on $\Im$ and the boundary condition $H = 0$ on the border of the union of surfaces A and Σ.

The non-linear theoretical problem of a thin airfoil in an unsteady flow is then rigorously settled. The wake shedding is described by the relative shedding velocity, which determines the shedding direction of the vortex particles, and by the Kutta–Joukowsky condition, which determines the contravariant components of the vortex density (or the discontinuity potential) shed in the wake. The variable-geometrical shape of the wake is governed by the wake time variation equation for the vortex particle $(\vec{\varpi}, \vec{\gamma})$. Equations (24), (26), (27) and (29) form a non-linear integro-differential system to be solved and its solution requires a numerical approach.

In many usual configurations, the wake shedding can satisfactorily be prescribed on the shedding edge flight path. In this case, $\vec{V}_{\text{re}}$ can be assumed to be equal to the flight path velocity of $\Im$, i.e.

$$\vec{V}_{\text{re}} = -\frac{\partial \vec{h}}{\partial t}. \tag{30}$$

Thus, the integro-differential system solution can be simplified, because $\vec{V}_{\mathrm{re}}$ is no longer an unknown. This assumption does not allow us to compute a wake shedding from a leading edge, or from airfoil tips, but it is very suitable in the case of a trailing edge.

The pressure jump can be computed using the Bernoulli equation (23) in the airfoil-fixed system of reference. The pressure difference across the airfoil is then

$$\frac{\Delta p}{\rho} = \frac{p^- - p^+}{\rho} = \frac{1}{2}(\vec{U}^{+2} - \vec{U}^{-2}) + \frac{\partial[\varphi]}{\partial t} + \vec{V}_E \cdot [\vec{U}]. \tag{31}$$

Therefore, in terms of the median velocity $\vec{U}^* = (\vec{U}^+ + \vec{U}^-)/2$, and of the discontinuity potential K, Equation (31) becomes

$$\frac{\Delta p}{\rho} = (\vec{U}^* + \vec{V}_E) \cdot \vec{\nabla} K + \frac{\partial K}{\partial t}. \tag{32}$$

Knowing the pressure and the potential field, we can compute the forces and moments, as well as all the desired flow characteristics, such as surface velocity surveys.

The total force obtained by this pressure difference integration does not account for the leading-edge suction force. This force is a direct consequence of the singularity occurring at the leading-edge in the case of a thin airfoil, and mainly contributes to the drag force. Apart from its formulation by Blasius' formulas in steady 2D flow, few works deal with this force computation in a more general framework.

The general problem of the non-linear unsteady 3D inviscid flow around a lifting–propulsive system is then completely and rigorously formulated. The shedding and deforming is formulated explicitly for the wake, so that it will be possible to simulate the distorted wake. This general theory provides the basis for a straight discretization and for a numerical method of solution.

4. DISCRETE FORMULATION AND NUMERICAL METHOD OF SOLUTION

The discrete scheme and the numerical method presented in this section constitute one possible implementation of the theory presented above, the aim of which is to demonstrate that such an approach provides a competitive code in terms of computing costs and versatility.

4.1. Discretization of geometrical surfaces

Discretization of the two geometrical surfaces, A and Σ, is performed in the definition planes of their respective parametrisations $\vec{\chi}$ and $\vec{\varpi}$. Hence the approximations of $\vec{\chi}$ and $\vec{\varpi}$ are defined in relation to a subdivision of their respective definition planes. The simplest possibility is to approximate the definition planes by the union of small uniform quadrilateral panels, as shown in Figure 5, and to approximate $\vec{\chi}$ and $\vec{\varpi}$ by their values at the center of these panels. These approximate values of $\vec{\chi}$ and $\vec{\varpi}$ are then the control or collocation points, where discrete equations are solved.

With the help of the parametrisations, it is possible to build an irregular distribution of airfoil points. For example, in the case of the airfoil, the airfoil tips, the leading edge and geometry discontinuities are regions of large flow characteristic variations. Under this condition, the precision of the results can be improved by using a suitable variable point spacing.

4.2. Discretization of a doublet distribution

In the present study, a step distribution of the discontinuity potential H over the panels was first considered. Referring to Equation (10), this distribution is equivalent to a vortex ring distribution in the definition planes of $\vec{\chi}$ and $\vec{\varpi}$; i.e. in Equation (10), only the curvilinear integral has to be approximated. Therefore the velocity is the one induced by a vortex ring singularity distribution, e.g. References [1] and [15]. Consequently, this type of approximated distribution is not very different from a classical vortex lattice approach, except that the discretization is performed in the parametrisation planes instead of the physical plane. In terms of induced velocity, it is well-known that such a low-order discretization model offers good results and, according to Reference [3], is sufficient to predict airload accurately. For this vortex ring model, an approximation of the parametrisation is needed at the corner of the panels. This is easily obtained from the collocation points, using a classical interpolation scheme. This discretization model has been retained for the vortex sheet representing the airfoil. But for the wake, it is necessary to use the vortex particle concept in order to deal with its time variation and deforming.

The velocity induced by a continuous distribution of vortex particles over Σ is

$$\vec{U}(x,t)=\frac{1}{4\pi}\iint_{\Omega}\frac{\vec{\gamma}\wedge\vec{r}(\vec{x},\vec{\varpi})}{r(\vec{x},\vec{\varpi})^3}\,\mathrm{d}q\,\mathrm{d}\tau-\frac{1}{4\pi}\int_{\partial\Omega}G\,\vec{\mathrm{grad}}_x\left(\frac{1}{r}\right)\wedge\mathrm{d}\vec{\xi}. \tag{33}$$

The curvilinear integral depends on the condition at the border of Σ, and can be approximated by a vortex ring there, whereas the surface integral has to be approximated over the entire surface Σ. A discrete vortex particle concept is introduced. One possible way to define this is to consider a step distribution of the contravariant components γ^{α} $(\alpha=1,2)$ of the vortex density over the panels. Hence, a discrete vortex particle scheme is derived from this approximation and that of the parametrisation $\vec{\varpi}$. Using i, j as indexing letters referring to a panel (i chordwise and j spanwise), the velocity induced by the vortex particle ij is

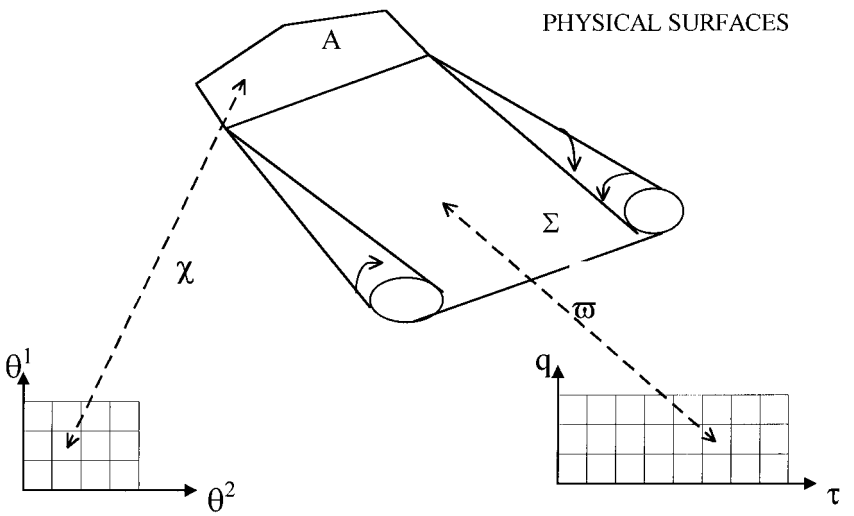

Figure 5. Discretisation of geometrical surfaces.

$$\vec{U}(x) \approx h^1 h^2 \gamma_{ij}^q \frac{(\partial \vec{\varpi}/\partial q)_{ij} \wedge (\vec{x} - \vec{\varpi}_{ij})}{\|\vec{x} - \vec{\varpi}_{ij}\|^3} + h^1 h^2 \gamma_{ij}^\tau \frac{(\partial \vec{\varpi}/\partial \tau)_{ij} \wedge (\vec{x} - \vec{\varpi}_{ij})}{\|\vec{x} - \vec{\varpi}_{ij}\|^3}, \tag{34}$$

where h^1 and h^2 are, respectively, the chordwise and spanwise increments of the discrete plane (q, τ). In Equation (34), the ϖ-derivates referring to the definition plane must be approximated. A finite difference scheme is suitable. The velocity induced by a discrete vortex particle distribution is therefore

$$\vec{U}(x) \approx \sum_{ij} h^1 h^2 \left(\gamma_{ij}^q \frac{(\partial \vec{\varpi}/\partial q)_{ij} \wedge (\vec{x} - \vec{\varpi}_{ij})}{\|\vec{x} - \vec{\varpi}_{ij}\|^3} + \gamma_{ij}^\tau \frac{(\partial \vec{\varpi}/\partial \tau)_{ij} \wedge (\vec{x} - \vec{\varpi}_{ij})}{\|\vec{x} - \vec{\varpi}_{ij}\|^3} \right). \tag{35}$$

It is well-known that any discretization of this type (vortex ring, discrete vortex particle) introduces a fluid velocity singularity, although the continuous formulation does not present such a singular behavior. This is the case here, as $\vec{x}$ tends to the vortex particle point, i.e. when r tends to zero. In order to avoid numerical divergence and thereby regularize the singular behavior of the velocity field, this discrete vortex particle model requires a 'regularization' radius rc, which has to be defined. According to Reference [6], the regularization process retained in the present work, consists of multiplying the induced velocity by the coefficient $r^2/(r^2 + rc^2)$.

Numerical tests have shown that, whereas the discrete vortex particle model is particularly well suited for the unsteady deforming wake prediction, the vortex ring model was more accurate concerning the near-field induced velocity prediction, especially when the flow tangency condition is applied. This is why, in the present study, a double-discretization has been used for the vortex sheet representing the wake, in the definition plane of $\vec{\varpi}$:

– the vortex ring model to solve the flow tangency condition,
– the discrete vortex particle model to solve the evolution equation.

Therefore, each panel is associated with a vortex ring or a vortex particle. Changing the discretization model increases computing time costs very slightly but it yields very good computational capabilities, especially for simulating wake geometry deformation and time variation.

A theoretical formulation is available, therefore it is quite possible to think of other schemes of higher order approximation to improve the velocity field computation.

4.3. Numerical method

The numerical scheme is based on a time stepping procedure. The study time interval $[0, T]$ is divided into small time intervals Δt. At the initial instant $(t = 0)$, no wake exists. At each time step including the first one, the airfoil is moved along its flight path and the wake from the shedding edge can be predicted from the corresponding set of discrete equations of Section 3.2.

At each time step, the local velocity at each control point on the airfoil has to satisfy the flow tangency condition (24), where the local velocity is the resulting velocity induced by the combination of the vortex ring distribution in the definition planes of $\vec{\varpi}$ and $\vec{\chi}$, modeling the airfoil and its wake. At this stage, the unknowns are the strengths of the airfoil vortex ring elements and the characteristics of the vortex ring elements currently being shed. The position of each of the other wake vortex ring elements has been determined by solving the wake time variation equation during the previous time step, and its strength by the Kutta–Joukowsky condition, when shed.

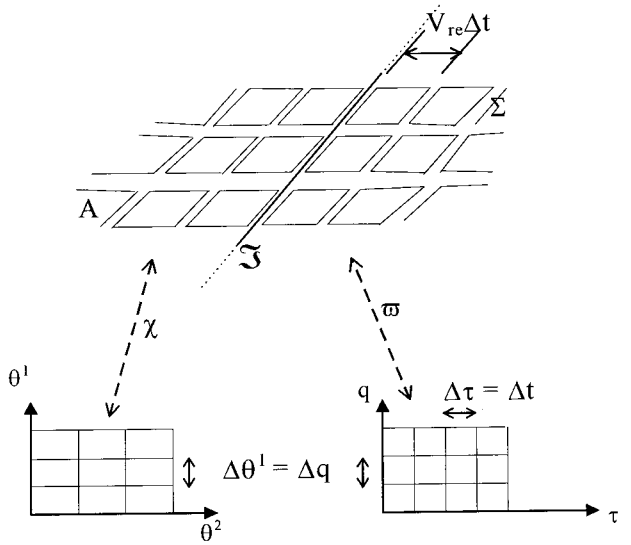

Figure 6. Distribution of airfoil and wake vortex ring elements at the shedding edge $\Im$.

At each time step, the wake strip shed during the current time step is a row of free vortex ring elements, as shown in Figure 6. Their positions must be calculated by the shedding process. This shedding process is governed by two coupled equations, the Kutta–Joukowsky condition and the time variation equation. To find the solution, an iterative numerical approach is generally needed. But, in the present work, the position of these vortex ring elements is derived directly from the shedding assumption $\vec{V}_{re} = -\partial\vec{h}/\partial t$. Thus, in the physical domain, they correspond to the interval covered by the trailing edge during the time step. Their strengths are determined by applying the Kutta–Joukowsky condition. With the assumptions referring to the discretization, condition (ii) of the Kutta–Joukowsky condition (21) disappears and only the continuity condition of H across $\Im$ remains. In this case, the discrete Kutta–Joukowsky condition then consists of setting the strengths of the vortex ring elements equal on both sides (airfoil and wake) of the trailing edge.

Using the wake shedding procedure, the discretization of the flow tangency equation (24) derived at the control points yields to the following set of algebraic equations:

$$\begin{bmatrix} \cdot & \cdot & \cdot \\ \cdot & A_{k,l} & \cdot \\ \cdot & \cdot & \cdot \end{bmatrix} \begin{pmatrix} K_1 \\ K_2 \\ \cdot \\ \cdot \\ K_M \end{pmatrix} = \begin{pmatrix} \cdot \\ \cdot \\ B_1 \\ \cdot \\ \cdot \end{pmatrix} + \begin{bmatrix} \cdot & \cdot & \cdot \\ \cdot & C_{i,j} & \cdot \\ \cdot & \cdot & \cdot \end{bmatrix} \begin{pmatrix} G_1 \\ G_2 \\ \cdot \\ \cdot \\ G_N \end{pmatrix}, \tag{36}$$

where M and N refer to the number of unknown and known elements respectively. On the left-hand-side are the unknowns $K_{l=1,\ldots,M}$, which are the strengths of the airfoil vortex ring elements, and which take into account the strengths of the currently shed vortex ring elements due to the Kutta–Joukowski condition. $A_{k,l}$ is the velocity influence coefficient, representing the velocity at the control point k due to the airfoil vortex ring element l and the wake shedding vortex ring elements. The terms on the right-hand-side are known. B_1 represents the velocity at the control point k due to the kinematic and deformation motion of the airfoil, and

$C_{i,j}$ the velocity due to the known wake vortex ring elements. Note that N increases with each additional time step. $A_{k,l}$ and $C_{i,j}$ are complex relations, and their derivation is documented in Reference [15]. At each time step, the solution of Equation (36) can be obtained by inverting the matrix A of the influence coefficient. If the shape of the airfoil remains unchanged, the matrix inversion occurs only once. When the strengths $K_{l=1,\ldots,M}$ are known, the resulting aerodynamic loads, forces and moments can be computed.

The discretization of the time variation equation requires a velocity field approximation, from the vortex ring model for the airfoil and from the discrete vortex particle model for the wake. Its solution gives the new position of the vortex particles at each time step. The contravariant components of $\vec{\gamma}$ are computed from the approximation of G, which has been determined once for all at the shedding time by the Kutta–Joukowsky condition. This solution is obtained here using a Runge–Kutta algorithm. The resolution order of the algorithm depends both on computation time and accuracy to predict the wake geometry. The higher the order, the better the wake roll-up is simulated. After several numerical tests, a second-order algorithm was chosen.

5. RESULTS

5.1. Convergence of the numerical process

One part of this work [15] was to carry out some numerical experiments on simple configurations in order to test the convergence of the numerical process more precisely in relation to the discretization parameters, such as the time step and the number of airfoil panels, chordwise and spanwise. The results have shown that the different numerical schemes behave quite well. In every case, convergence was obtained by improving the discretization refinement (increasing the number of airfoil panels chordwise and spanwise and decreasing the time step). For example, Figure 7 illustrates the effect of the reduced time step $\Delta\tilde{t} = U_\infty \Delta t/c$ (c

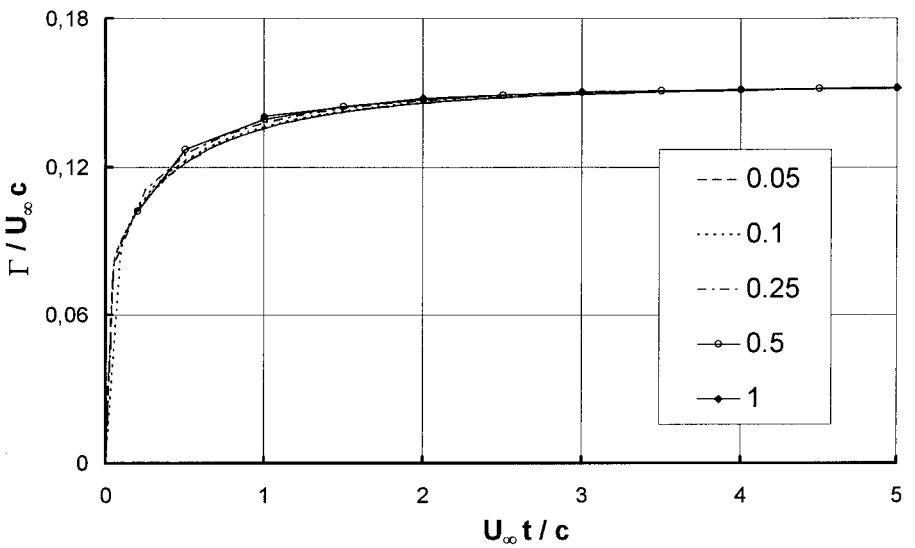

Figure 7. Effects of the reduced time step $\Delta\tilde{t}$ on the circulation time variation.

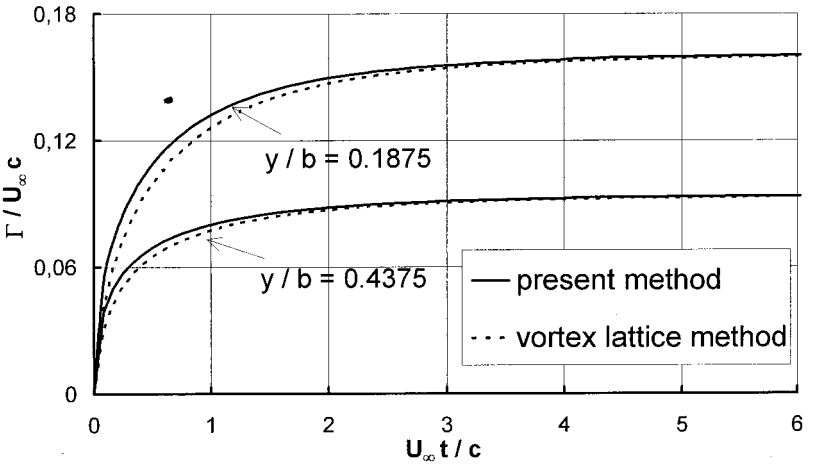

Figure 8. Sectional circulation time variation of a rectangular planform ($AR = 3$), sudden setting at incidence of 5°.

being the mean airfoil chord) on the time variation of the reduced circulation $\Gamma/U_\infty c$ (Γ corresponds to $[\phi]$ at the trailing edge), at the section $y/b = 0.1875$ (b is the span) of a rectangular planform airfoil, with an aspect ratio $AR = 3$. The motion is a sudden setting of the airfoil to 5° of incidence in forward flight at a constant speed U_∞, from an initial incidence of 0°. The airfoil is divided into four equally spaced chordwise elements and 40 spanwise. Figure 7 shows a solution that may be considered as converged (i.e. Γ hardly changes as the time step decreases), even with quite large time-step values. This offers interesting prospects in terms of reduction of computation run-time.

Unless otherwise stated, the results presented below are considered to be converged in relation to these discretization parameters.

5.2. Comparison of results

Some comparisons were made of our results with those obtained by a classical vortex ring approach, developed according to Reference [1], and with those obtained by Djodjodihardjo and Widnall [3]. Only those results obtained for the time variation of the sectional circulation for rectangular planforms ($AR = 3$ or 6) are presented here for the two following unsteady motions:

- sudden setting of the airfoil at incidence in a constant speed forward flight U_∞, from an initial incidence of 0° (Figures 8 and 9),
- vertical sinusoidal heaving oscillations of the airfoil with reduced period $\tilde{T} = U_\infty T/c = 5$ and with amplitude $A = \pm 0.087 U_\infty T$ (Figure 10).

As was the case in all the comparisons, Figures 8–10 show a satisfactory agreement between the present method and the others. Moreover, the computation times are equivalent.

5.3. Application to flapping variable-geometry wings

To illustrate the capabilities of the present method to solve non-linear unsteady lifting potential flow problems for wings of variable geometry, we present the calculation of flapping wings of variable geometry. This case is based on works about the forward flight of birds [16,17].

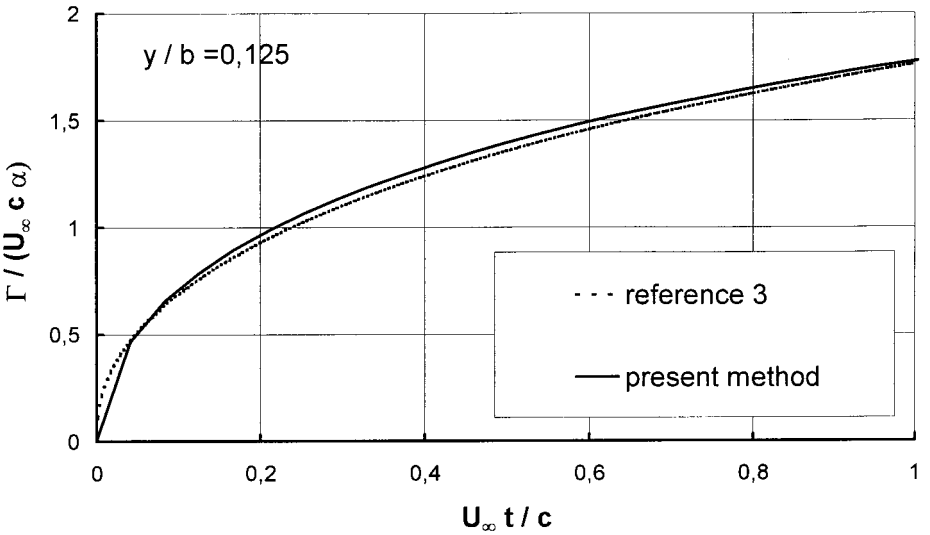

Figure 9. Sectional circulation time variation of a rectangular planform ($AR = 6$), sudden setting at incidence of 17°.

Consider a pair of flapping wings flying with a constant forward velocity $\vec{U}_0$ and hinged about a longitudinal axis x. The planform used in all the calculations is described in Figure 11. The chord is constant along the inner half of each wing, and parabolically decreasing along the outer half:

$$c(y) = \begin{cases} c_o & \text{for } 0 < y \leq \dfrac{b}{4} \\ 16 c_o \dfrac{y}{b}\left(\dfrac{1}{2} - \dfrac{y}{b}\right) & \text{for } \dfrac{b}{4} < y < \dfrac{b}{2} \end{cases} \tag{37}$$

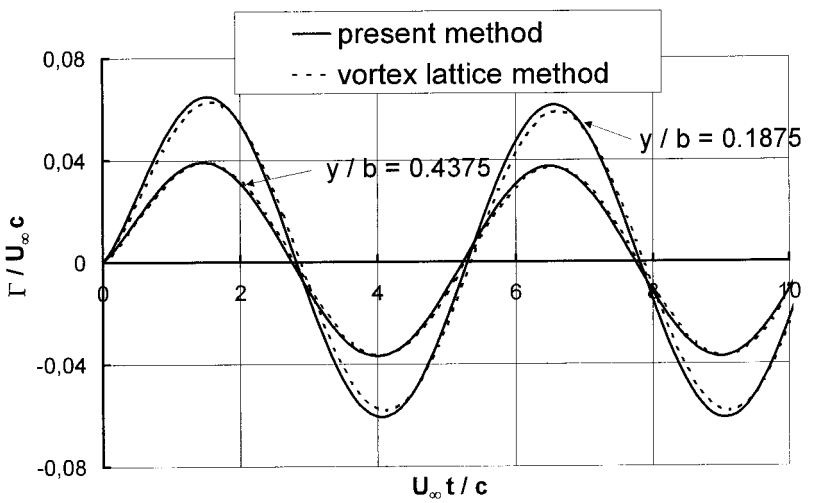

Figure 10. Sectional circulation time variation. Sinusoidal heaving oscillations of a rectangular planform ($AR = 3$).

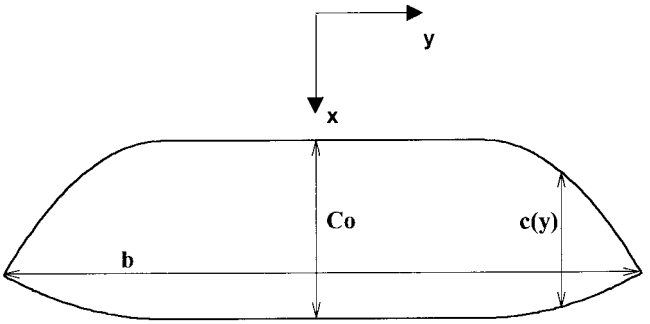

Figure 11. Flapping wing planform.

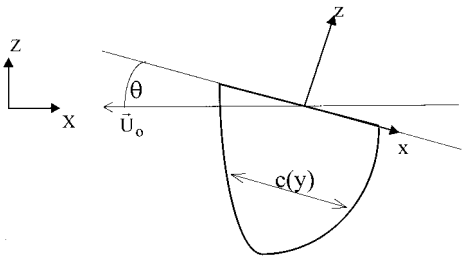

Figure 12. Flapping plane.

The aspect ratio is 7.13. This planform shape is a good approximation of that of a pigeon.

The angle between the longitudinal axis and the flight path is θ, as shown in Figure 12. The wings flap in a plane perpendicular to this axis. The total angular amplitude of flapping is $\phi_{\max}$. The instantaneous angle between the wing and the horizontal is $\phi(t)$, as shown in Figure 13. The angular flapping velocity is $\dot{\phi}(t)$.

The flapping motion is periodic, and one complete period consists of a downstroke, an upstroke and two transient motions. The length of the upstroke and the downstroke are chosen to be equal. According to References [15] and [16], the downstroke produces lift and thrust, whereas lift and drag are at their smallest during the upstroke. Using T to describe the period length, $\varepsilon T/2$ is the length of a transient motion. The assumption of constant angular velocity of flapping $\dot{\phi}$ is applied during the upstroke and the downstroke. $\dot{\phi}$ is given by

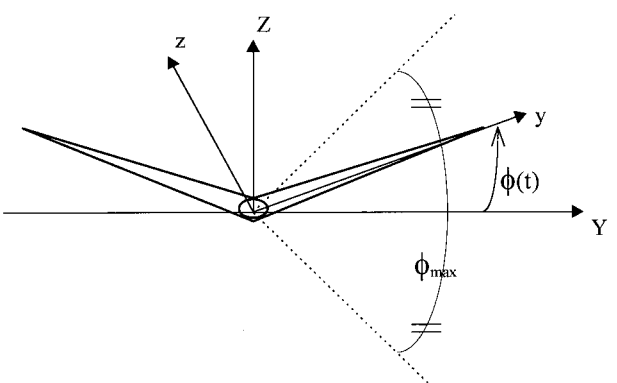

Figure 13. Flapping angle.

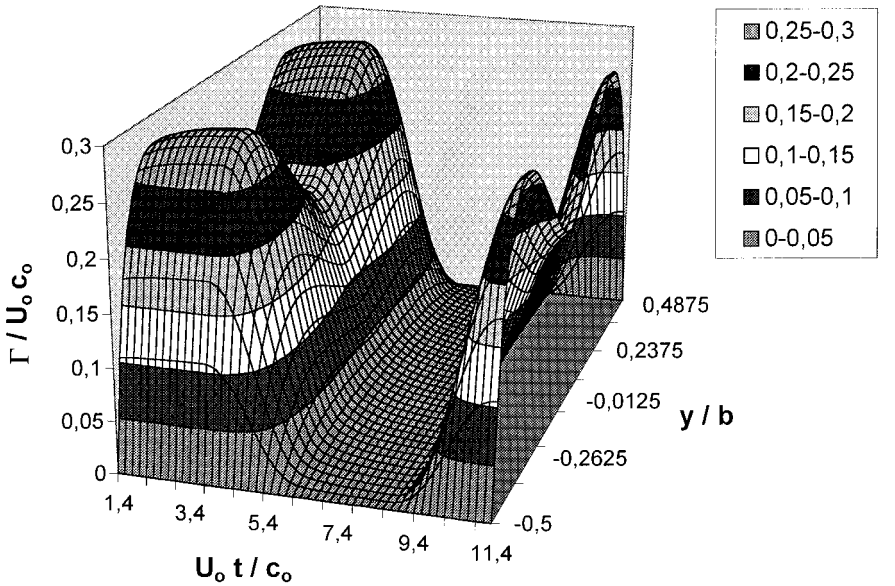

Figure 14. Spanwise and time variations of the circulation.

$$\dot{\phi}_{\mathrm{u}} = \frac{2\phi_{\max}}{T(1-\varepsilon)}, \qquad \dot{\phi}_{\mathrm{d}} = -\frac{2\phi_{\max}}{T(1-\varepsilon)}. \tag{38}$$

During the transient motions, ϕ has a sinusoidal variation.

In order to prevent unrealistic geometrical incidences, which result from the combination of the forward and flapping motions, it is necessary to introduce a wing twist. This twist is such as the resulting geometrical incidence does not exceed a set incidence $\alpha_{\max}$ during the downstroke, and is zero during the upstroke. The twist is then respectively given by

$$\alpha(y,t) = \alpha_{\max} - \arctan\left(\frac{-\sin\theta + \dot{\phi}_{\mathrm{d}} y}{-\cos\theta}\right), \qquad \alpha(y,t) = -\arctan\left(\frac{-\sin\theta + \dot{\phi}_{\mathrm{u}} y}{-\cos\theta}\right). \tag{39}$$

During the transient motions, these twists are connected through a sinusoidal arc. Numerical tests were run, which showed that the best results about thrust were obtained with a twist rotation axis defined as the three-quarter line chord. This is why the three-quarter line chord is rectilinear in the planform shape.

The motion parameters are $\tilde{T}$, a reduced flapping period, ε, θ, $\phi_{\max}$ and $\alpha_{\max}$. The following numerical results are obtained with the following parameters:

$$T = \frac{10c_o}{U_\infty}, \qquad \varepsilon = 0.5, \qquad \theta = 0^{\circ}, \qquad \phi_{\max} = 80^{\circ}, \qquad \alpha_{\max} = 20^{\circ}.$$

For the wake geometry computation, the wings were divided into four equally spaced chordwise elements and 30 spanwise, and the time step is $U_o \Delta t / c_o = 0.5$. The airload prediction required a more refined discretization. For the airload computation, the wings were divided into ten equally spaced chordwise elements and 40 spanwise, and the time step is $U_o \Delta t / c_o = 0.2$. The regularization radius rc has been chosen as satisfactorily low as $0.01 c_o$. For 2.5 periods, the computation run-time values were ≈ 20 min and 10 h, respectively, on a Pentium 120 MHz personal computer. These values have been obtained without any particular optimization of computation run-time.

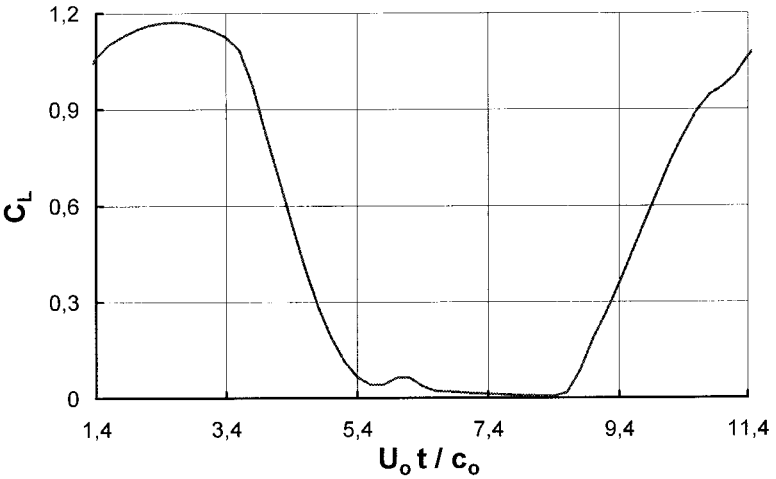

Figure 15. Lift coefficient time variation.

Figure 14 shows the spanwise variation with time of the circulation, and Figures 15 and 16 exhibit the variation of the lift and thrust–drag coefficients, respectively, throughout one complete period of flapping motion. C_D and C_L are defined as

$$C_D = \frac{D}{\frac{1}{2}\rho S U_\infty^2}, \qquad C_L = \frac{L}{\frac{1}{2}\rho S U_\infty^2}, \tag{40}$$

where D and L are, respectively, the components of the aerodynamic force parallel and perpendicular to the flight direction described by $\vec{U}_\infty$, and S is the untwisted planform area. These numerical results show the desired characteristics. Lift and thrust ($C_D < 0$) are essentially produced on the downstroke, whereas the lift and drag are negligible on the upstroke. The twist may not be optimal in relation to the flapping motion, as a peak of drag coefficient

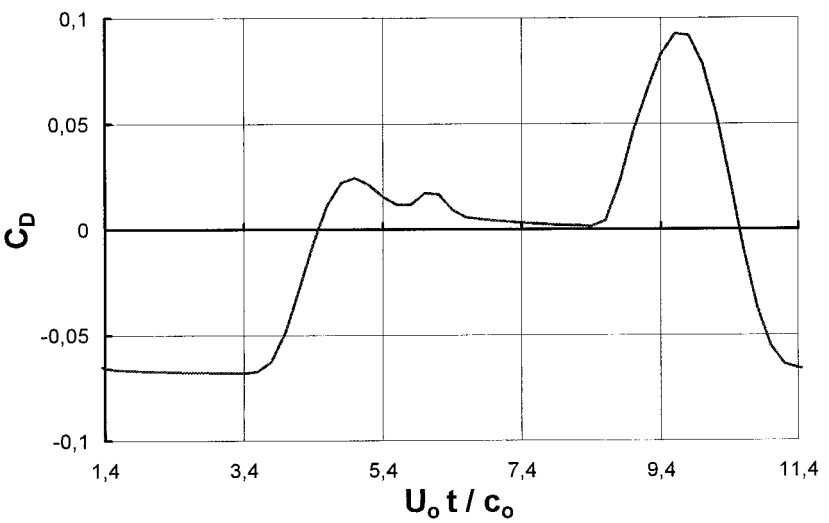

Figure 16. Thrust/drag coefficient time variation.

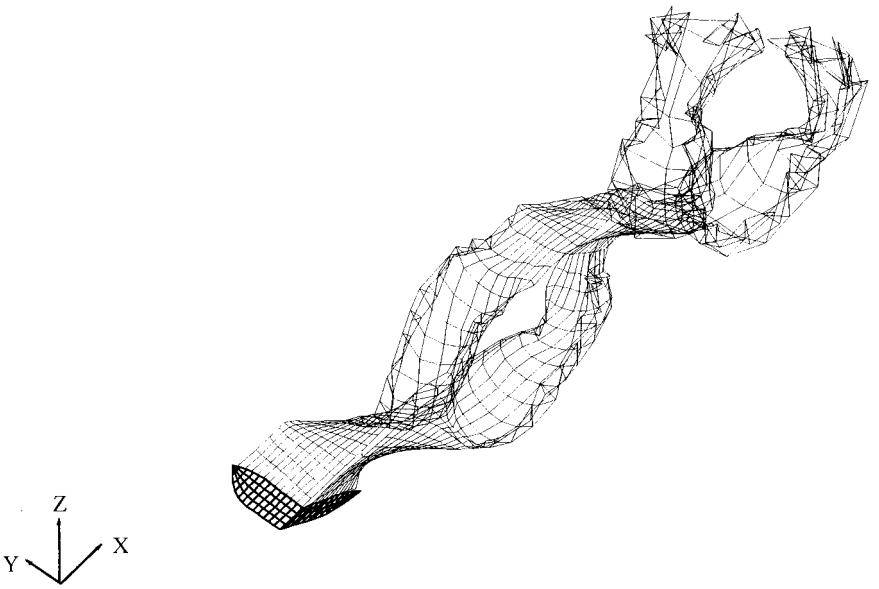

Figure 17. Wake geometrical shape at $\tilde{t} = U_o t/c_o = 20$.

appears during the second transient motion. Figure 17 displays the wake geometrical shape at the reduced time $\tilde{t} = U_o t/c_o = 20$ after 2.5 calculated periods. In the distorted wake, the tip roll-ups can be clearly noted.

6. CONCLUSIONS

On a basis of a rigorous and complete continuous theoretical formulation, a numerical method has been developed to solve the unsteady 3D aerodynamics of lifting–propulsive systems. Computational simulations were performed to validate this present approach.

The theory leads to a view of the vortex wake similar to that of a classical vortex lattice approach, but using a discrete vortex particle concept, which is particularly well suited for the unsteady deforming wake computation. This discrete vortex particle concept is not very far from the one developed by Rehbach. However, it is founded on another theoretical basis, leading to a simpler method of solution. Two main points have actually contributed to reducing computational costs and improving flexibility compared with the vortex particle methods. The first is the number of unknowns concerning the vortex particle at each time step in the wake. The only unknown in the present method is the particle position, whereas the particle position and strength are both unknown in the usual vortex particle method. Then the second point concerns the algorithms used to solve the time variation equation. In fact, the present method allows a treatment of wake deformations comparable with the vortex particle methods, but without their limitations, and compares with classical vortex lattice approaches in terms of computing costs. This method is even more flexible than the latter as far as the choice of discretization parameter values are concerned.

The present method provides a basis for a more accurate treatment of more difficult problems. At this stage of development, the method allows the treatment of wakes issued from only the trailing edge because of the assumption described in Section 2.3. However, the general theory allows wake shedding from any shedding line.

Moreover, as this numerical approach stems from a complete theory, it is possible to approximate the wake (geometry and doublet distribution) with other more precise discrete schemes, such as a linear approximation of the discontinuity potential over the panels. An approximation, having similarities with a finite element approach, is currently being studied. It is also possible to switch from a refined discretization level to a less refined one, or inversely during the computation, so that the near and far velocity inductions can be dealt with differently.

Another development of this method is also to consider wake–wake and wake–body interactions in a multi-element system, such as rotor blades. For such high aspect ratio systems, we are now concentrating on associating the present unsteady wake model with an unsteady lifting line model for the blades, such as in the recent work of Devinant [18].

REFERENCES

1. J. Katz and A. Plotkin, *Low Speed Aerodynamics—From Wing Theory to Panel Methods*, McGraw Hill, New York, 1991.
2. E. Albano and W.P. Rodden, 'A doublet-lattice method for calculating lift distributions on oscillating surfaces in subsonic flows', *AIAA J.*, **7**, 279–285 (1969).
3. R.H. Djodjodihardjo and S.E. Widnall, 'A numerical method for the calculation of non-linear, unsteady lifting potential flow problems', *AIAA J.*, **7**, 2001–2009 (1969).
4. J. Katz and B. Maskew, 'Unsteady low-speed aerodynamic model for complete aircraft configurations', *J. Aircr.*, **4**, 302–310 (1988).
5. D.T. Mook, 'Unsteady aerodynamics', *Lectures*, *Von Karman Institute for Fluid Mechanics*, 1988.
6. B. Michea, 'Etude des sillages de rotors d'hélicoptère en vol d'avancement et de leur influence sur les performances du rotor', *Thèse Doctorat*, Paris VI, 1992.
7. C. Rehbach, 'Calcul numérique d'écoulements tridimensionnels instationnaires avec nappes tourbillonnaires', *La Rech. Aérosp.*, **5**, 289–298 (1977).
8. Y. Morchoisne, 'Calcul d'écoulements instationnaires par la méthode des tourbillons ponctuels', *AGARD Advis. Rep.*, **239**, (1986).
9. S. Huberson, 'Calculs d'écoulements tridimensionnels instationnaires incompressibles par une méthode particulaire', *J. Méc. Théor. Appl.*, **3**, 805–819 (1984).
10. G.S. Winckelmans and A. Leonard, 'Contributions to vortex particle methods for the computation of three-dimensional incompressible unsteady flows', *J. Comput. Phys.*, **109**, 247–173 (1993).
11. M. Mudry, 'La Théorie générale des nappes et filaments tourbillonnaires et ses applications à l'aérodynamique instationnaire', *Thése de Doctorat d'Etat*, Paris VI, 1982.
12. M. Mudry, 'Théorie explicite de la couche médiane associée à une nappe tourbillonnaire', *Note au CRAS Paris*, **296**, 1109–1112 (1983).
13. M. Mudry, 'Fondements d'une théorie générale des sillages instationnaires considérés comme des nappes tourbillonnaires', in *Actes du 6ème Cong. Français de Mécanique*, Thème **26**, 5–8 (1983).
14. A. Leroy, M. Mudry and Ph. Devinant, 'Sur la condition de Joukowsky en écoulement tridimensionnel', in *Actes du 12ème Cong. Français de Mécanique*, **III**, 165–169 (1995).
15. A. Leroy, 'Une méthode générale de calcul des systèmes portents et/ou propulsifs minces', *Thèse Doctorat*, Orléans, 1997.
16. R.J. Philips, R.E. East and N.H. Pratt, 'An unsteady lifting line theory of flapping wings with application to the forward flight of birds', *J. Fluid Mech.*, **112**, 97–125 (1981).
17. J.M.V. Rayner, 'A vortex theory of animal flight—Part I and Part II', *J. Fluid Mech.*, **91**, 697–730 (1979).
18. Ph. Devinant, 'An approach for an unsteady lifting-line time-marching numerical computation', *Int. J. Numer. Methods Fluids*, **26**, 177–197 (1998).

